LIMNOLOGY and OCEANOGRAPHY

ASLO

Limnol. Oceanogr. 9999, 2022, 1–11

doi: 10.1002/lno.12151

The effects of Ni availability on H_2 production and N_2 fixation in a model unicellular diazotroph: The expression of hydrogenase and nitrogenase

Hsin-Ting Li [1], **Sing-how Tuo** [1], **Mei-Chen Lu** [1], **Tung-Yuan Ho** [1,2*]

[1]Research Center for Environmental Changes, Academia Sinica, Taipei, Taiwan
[2]Institute of Oceanography, National Taiwan University, Taipei, Taiwan

Abstract

We investigated the effects of Ni concentration on hydrogen (H_2) net production and nitrogen (N_2) fixation rates in a model unicellular diazotrophic cyanobacterium, *Cyanothece*. We quantified NiFe uptake hydrogenase of the diazotroph to examine how Ni deficiency affects the expression of hydrogenase and nitrogenase and N_2 fixation rates. We found that Ni availability controls its H_2 net production and the expression of HupL, the major subunit of the uptake hydrogenase. Low Ni availability induced low HupL expression levels while yielding high H_2 net production, and vice versa. We also identified the threshold range of Ni concentrations that may differentiate low and high H_2 net production patterns in the diazotroph. However, the substantial variations in Ni availability and H_2 net production did not affect nitrogenase expression and N_2 fixation rates in *Cyanothece*. From two independent studies in the Atlantic tropical and subtropical oceans, we found that dissolved Ni concentrations and H_2 oversaturation percentage exhibited a statistically significant negative correlation, which is consistent with the findings of this culture study. Overall, these results indicate that Ni availability may affect H_2 net production and concentrations in the euphotic zone of the oceanic regions. H_2 concentrations may be used as a promising proxy to reflect N_2 fixation activities in tropical and subtropical oceans only under Ni-deficient conditions.

Early studies reported that supersaturated H_2 concentrations are widely observed in the surface waters of tropical and subtropical oceans (Herr and Barger 1978; Setser et al. 1982). Later studies have shown strong correlation between excessive H_2 concentrations and N_2 fixation rates, confirming that supersaturated H_2 mainly originates from the production of diazotrophic phytoplankton (Scranton 1984; Moore et al. 2009, 2018). However, both field and laboratory studies have indicated that the molar ratios of H_2 net production rates to N_2 fixation rates are not equal to 1. Theoretically, the ratio should be equal to 1 due to the following reaction:

$$1N_2 + 16ATP + 8H^+ + 8e^- \rightarrow 2NH_3 + 1H_2 + 16P_i + 16ADP.$$

Both field and laboratory studies have demonstrated that the molar ratios are much smaller than 1, ranging from 0.003 to 0.48 (Schropp et al. 1987; Punshon and Moore 2008; Wilson et al. 2010). Intracellular H_2 removal is considered to be the main cause of these highly varied ratios. H_2 is oxidized to protons and electrons due to the uptake of hydrogenase in diazotrophic cyanobacteria to generate reducing equivalents such as NADPH and to drive electron transfer chains in ferredoxin or cytochrome, which may enhance Fe uptake or ATP production for N_2 fixation in cells (Dixon 1972; Bothe et al. 2010; Eichner et al. 2019). When H_2 produced by N_2 fixation is not utilized by uptake hydrogenase, it is released into the ambient seawater, causing supersaturation, particularly under low mixing conditions. Since Ni serves as an essential cofactor in NiFe uptake hydrogenase to bind H_2 at its active site for H_2 oxidation (Volbeda et al. 1995), Ni availability would affect cellular H_2 net production in diazotrophic phytoplankton. Previous laboratory studies on freshwater diazotrophs using reverse transcription polymerase chain reaction have reported that high-level Ni addition leads to high expression of *hupL* transcripts, while Ni-depletion treatment revealed high H_2 net production (Daday and Smith 1983; Daday et al. 1985; Axelsson and Lindblad 2002). However, the Ni concentrations

*Correspondence: tyho@gate.sinica.edu.tw

Additional Supporting Information may be found in the online version of this article.

Author Contribution Statement: TYH, ShT, and HTL conceived and designed the study. HTL and MCL carried out the laboratory experiments. HTL, MCL, ShT, and TYH analyzed the data. TYH and HTL wrote the paper.

applied in these three freshwater studies ranged from 21 to 680, 17 to 170, and 500 nM, which are one to two orders of magnitude of the total dissolved Ni concentrations observed in the euphotic zone of tropical and subtropical oceans.

Total dissolved Ni concentrations are generally ~2 nM in the surface waters of tropical and subtropical oceans globally (Bruland 1980; Middag et al. 2020; Zheng et al. 2021). Compared with the Ni concentrations used in the three freshwater studies mentioned above, Ni concentrations of 2 nM are relatively low. However, in the surface water of the open ocean, the concentration level of 2 nM is approximately one order of magnitude higher than the total dissolved Fe concentrations, which normally exhibit values of 0.2–0.3 nM in the surface water of the open ocean. Due to its relatively high concentrations in the euphotic zone and potentially high bioavailability (Saito et al. 2004), Ni has not been regarded as a limiting factor for phytoplankton growth in oceans. However, some culture studies have indicated that Ni can be a limiting factor for some marine cyanobacteria or diazotrophs under specific growth conditions (Dupont et al. 2008; Ho 2013). The required Ni concentrations to satisfy cellular H_2 uptake in marine diazotrophs remain unclear.

To the best of our knowledge, there are three Ni enzymes in marine phytoplankton, including urease, Ni superoxide dismutase, and NiFe uptake hydrogenase. Previous studies on the Ni requirements of marine phytoplankton have mostly focused on the utilization of urea (Price and Morel 1991; Dupont et al. 2008). Later culture studies have found that the addition of nanomolar levels of Ni to natural seawater may enhance superoxide dismutase activities and the growth of *Trichodesmium* (Ho 2013; Rodriguez and Ho 2014). Besides Ni superoxide dismutase and urease, the effects of Ni availability on NiFe uptake hydrogenase in marine diazotrophs are poorly understood. For the first time, Tuo et al. (2020) applied trace metal-defined culture techniques at low nanomolar Ni concentrations to examine the effects of Ni availability on H_2 production and N_2 fixation in *Cyanothece*. They found that total dissolved Ni concentrations below 10 nM (with 20 μM ethylenediaminetetraacetic acid, EDTA) caused high H_2 net production. The authors suggested that high H_2 net production could be attributed to insufficient HupL expression under low Ni availability, and H_2 net production might affect N_2 fixation rates. Some previous studies presented contradicting arguments about the impacts of H_2 concentration on nitrogenase activity and N_2 fixation rates. Zhang et al. (2014) demonstrated that *hupL*-knockout *Cyanothece* exhibited no N_2 fixation or H_2 net production, and proposed that HupL may remove reactive oxygen species or O_2 to protect nitrogenase. Guth and Burris (1983) found that high deuterium partial pressure decreased N_2 fixation rates in *Klebsiella pneumoniae*, suggesting that H_2 may outcompete N_2 for nitrogenase reaction. Daday et al. (1985) reported that high H_2 net production had no negative impact on N_2 fixation in *Anabaena cylindrica*. Thus, the impacts of H_2 net production on nitrogenase or N_2 fixation in marine diazotrophs also require further investigation.

Given the absence of Ni superoxide dismutase and urease cellularly, the influence of Ni availability can be attributed to NiFe uptake hydrogenase in *Cyanothece*. *Cyanothece* is thus an ideal model diazotroph to study the effects of Ni availability on H_2 production and N_2 fixation in marine diazotrophs. This study quantified specific growth rates, H_2 net production rates, N_2 fixation rates, and the expression of HupL and NifH to elucidate the effects of various levels of Ni availability. We also examined the distribution patterns of Ni concentrations and H_2 supersaturation in the surface waters of tropical and subtropical oceans to confirm the results observed in this culture study.

Methods

Batch cultures of *Cyanothece* strain ATCC 51142 were grown in 1-L transparent polycarbonate Erlenmeyer flasks with 1 L of trace metal-defined modified YBC II culture medium (Ho 2013). The preparation procedures and sterilization of the medium were previously described in detail (Ho et al. 2003; Tuo et al. 2020). Before the addition of trace metals, background trace metal concentrations in the culture medium were measured and validated by using a high-resolution inductively coupled plasma mass spectrometer (ICPMS, Element XR, Thermo Fisher Scientific) (Ho et al. 2010; Wang et al. 2014). The background Ni concentration in the medium was nearly 0.03 nM, which is considered the concentration of the lowest Ni treatment in this study. Total dissolved Ni concentrations in the other three treatments were 0.20, 2.0, and 20 nM. The concentration conditions of the four treatments are shown as 0.03, 0.2, 2, and 20 nM. All the treatments were carried out in triplicate culture bottles, which were kept in an incubator at 27°C with an orbital shaking speed of 100 revolutions min^{-1}. The light intensity was set at ~400 $\mu E\ m^{-2}\ s^{-1}$ with a 12:12 h light–dark square wave cycle.

Two major experiments were conducted to evaluate the reproducibility and validate the reliability of the major parameters measured in this study. An additional experiment was conducted to evaluate the reproducibility of protein expression. H_2 net production and N_2 fixation rates were not measured in the additional experiment. In the two major experiments (denoted as the 1st and 2nd experiments hereafter), cell density and size were monitored by using a Beckman Multisizer 3 Coulter counter. Specific growth rates were determined by using the cell density data, which were collected during the exponential growth phase, generally ranging from 10^5 to 8×10^5 cells ml^{-1} (Supporting Information Fig. S1). In the exponential phase, cultures were harvested for the measurement of cellular trace metal quotas. The cells, filtered with 1 μm acid-washed polycarbonate filters, were digested at 120°C overnight in trace metal clean Teflon vials filled with 2 mL Milli Q water and 2 mL concentrated super-pure HNO_3

in the 1st experiment or with 2 mL of 80% super-pure HNO_3 and 20% of super-pure HF in the 2nd experiment. The digested samples were subsequently dried at 120°C, and then redissolved in 4 mL of super-pure 2 N HNO_3 for elemental analysis by ICPMS.

The diel observation of H_2 production and N_2 fixation was conducted at different diel periods in the 1st and the 2nd experiments. The 1st experiment was performed for 22 h from the starting time in the dark period (D0), while the 2nd experiment was performed for 30 h from the starting time during the light period (L0). *Cyanothece* is known to conduct N_2 fixation during dark periods. Initiations from the dark vs. light periods in the 1st and 2nd experiments may facilitate the evaluation of the uncertainty in the measurement of N_2 fixation at different illumination periods. The samples were collected during the exponential growth phase to measure various parameters, while H_2 net production and N_2 fixation were measured by using the mercury oxide (HgO) reduction technique (Schmidt and Seiler 1970) and acetylene (C_2H_2) reduction (Capone and Montoya 2001), respectively. Triplicate samples were prepared for individual cultures for each time point and assay. A culture sample (10 mL) was placed in a 20-mL vial crimp-sealed in a clean room. For the N_2 fixation assay, 2 mL of headspace gas from each vial was removed and replaced with 2 mL of C_2H_2. The vials used for both assays were incubated in the same incubator. The time course of incubation was initiated at D0, and the samples were collected at 0, 1, 5, 9, 13, and 22 h (D0, D1, D5, D9, L1, and L10) in the 1st experiment and at 0, 3, 9, 12, 15, 18, 21, 24, 27, and 30 h (L0, L3, L9, L12/D0, D3, D6, D9, D12/L0, L3, and L6) in the 2nd experiment. After the incubation, H_2 net production was measured by injecting the gaseous samples obtained from the H_2 production vials into a 0.1 mL sample loop of a Peak Performer 1 Reducing Compound Photometer (Peak Laboratories) equipped with a heated HgO bed and UV absorption detector. The samples for N_2 fixation were removed from the incubation vials, stored in 10-mL sealed vials, and subsequently measured by gas chromatography (Agilent 7890A) with a Poropak N column (Agilent, HP-PLOT Al_2O_3S). A 4 : 1 ethylene to fixed N_2 ratio was applied to convert N_2 fixation from ethylene production (Capone and Montoya 2001; Punshon and Moore 2008). H_2 net production and N_2 fixation rates were estimated by subtracting the value of a prior time point from the value obtained at any given time point and dividing by the time difference between the two time points. More detailed information about these measurements is provided by Tuo et al. (2020).

The expression of HupL and NifH proteins was measured by using western blotting (Burnette 1980). Culture samples (200–400 mL) were harvested around D5–D7 for each sample and subsequently concentrated by centrifugation at 13,000 rpm at 4°C for 10 min (Beckman Avanti® J-26 XP). The supernatant was removed, while the pellets were transferred into a microcentrifuge tube for further centrifugation at 13,000 rpm at 4°C for 5 min (Thermo FRESCO 17). The supernatant was removed, while the pellets were transferred to microcentrifuge tubes and frozen at −80°C until further processing. After adding protein extraction buffer (PEB AS08300, Agrisera) into the tubes, the cells were broken by using an ultrasonic probe for 3–4 rounds, with 10 s each round. The cells were cooled down on ice immediately after each round of sonication. The sonicated samples were subsequently centrifuged at 13,000 rpm for 10 min, while the supernatant was collected for the measurement of total protein concentration (Bio-Rad DC assay reagent). The sample was mixed with the buffer, beta-mercaptoethanol, and Laemmili, and heated at 95°C for 10 min. Six to nine micrograms of total protein was loaded in each sample lane on a TGX mini protean gel for electrophoresis at 200 V for 30–35 min (Bio-Rad). After electrophoresis, a stain-free image of the gel was captured by using a CCD camera-based imaging system (ChemiDoc MP; Bio-Rad). The proteins on the gel were transferred to an low-fluorescence polyvinylidene fluoride (LF-PVDF) membrane transfer system (Bio-Rad Trans-Blot® Turbo™). The transferred proteins were imaged to estimate the amount of total protein on the membrane for normalization. Then, the membrane was incubated in 5% skim milk in Tris-buffered saline with Tween 20 for blocking on an orbital shaker at 55–65 rpm for 1 h and incubated overnight at 4°C with primary antibodies against HupL or NifH. The HupL primary antibody design was customized by using the YNKKY KNSPF YEEAC sequence with a purity of 96% (Yao-Hong Biotechnology Inc.). We utilized *Thalassiosira oceanica* as a negative control to evaluate the specificity of the antibody against HupL (Supporting Information Fig. S2). NifH primary antibody was commercially available (AS01021A, Agrisera). After rinsing with TBS-T, the membranes were incubated with horseradish peroxidase (HRP) conjugated secondary antibodies (AS10653, Agrisera for HupL; AS101489, Agrisera for NifH). The secondary antibody was incubated at room temperature for 2 h on an orbital shaker at 55–65 rpm. The membrane was washed with wash buffer three times, for 10 min each wash, after incubation with both primary and secondary antibodies. Then, chemiluminescent signals were detected by using an imaging system after 5 min of incubation in ECL reagent (Bio-Rad). Total protein was utilized to normalize the chemiluminescence data for relative quantification of HupL or NifH in each experiment. Western blotting measurements were carried out using duplicate gels for each sample.

The responses (Ni quota, specific growth, H_2/N_2 ratio, and protein expression data) among different Ni treatments were compared by using one-way ANOVA and Tukey's studentized range post hoc test. Correlation analysis (Spearman's correlation) was performed for dissolved Ni and H_2 concentrations observed in the Atlantic Ocean, with the significance level (α) set at $p < 0.05$. All the data are presented as mean ± 1 standard deviation. All statistical procedures were carried out using R software version 4.1.0 (R Core Team 2021).

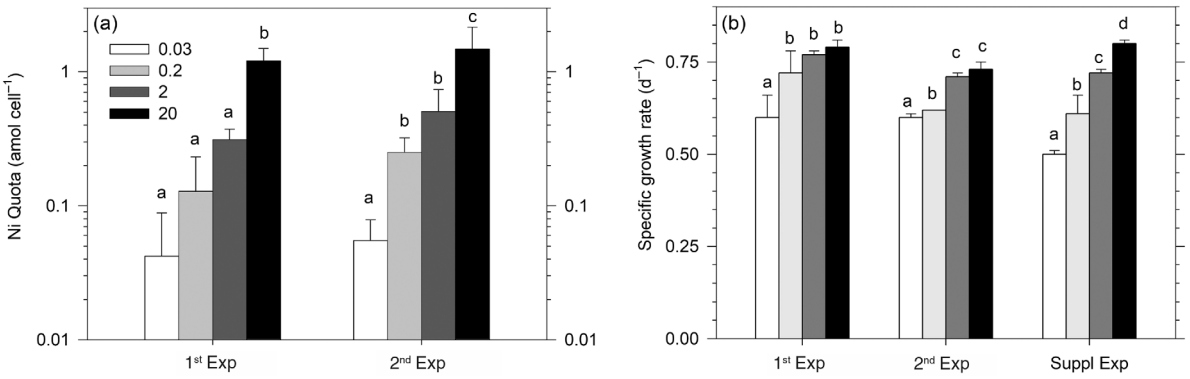

Fig. 1. Comparison of cellular Ni quota and specific growth rates among different Ni treatments. The bars of white, light gray, dark gray, and black represent the Ni treatments of 0.03, 0.2, 2, and 20 nM, respectively, and same for Figs. 2 and 3. Error bars stand for one standard deviation of data obtained from triplicate culture bottles for each treatment ($n = 3$), and same for Figs. 2 and 3. The letters shown above the bars represent the results of statistical tests among any paired treatments within the same experiment. Different letters stand for a significant ($p < 0.05$) difference among Ni treatments, and same for the following figures. (**a**) Ni quota obtained from 1st (ANOVA, $F_{3,8} = 35.0$, $p < 0.05$) and 2nd experiments (ANOVA, $F_{3,8} = 36.7$, $p < 0.05$). (**b**) Specific growth rates obtained from the 1st (ANOVA, $F_{3,8} = 11.2$, $p < 0.05$), 2nd (ANOVA, $F_{3,8} = 110.3$, $p < 0.05$), and supplementary experiments (ANOVA, $F_{3,8} = 135.3$, $p < 0.05$).

Results

It was found that the specific growth rates exhibited a slightly and significantly increasing trend in all the three experiments with increasing Ni concentrations (Fig. 1; Table 1; Supporting Information Fig. S1). This slight increase is potentially associated with sufficient expression of NiFe uptake hydrogenase, which can utilize H_2 to generate energy more efficiently. The effects on the growth rates were also reflected in the cell sizes, which decreased with increasing Ni concentrations and ranged from 58 ± 10 to 38 ± 2 μm^3 cell^{-1} (Table 1). The varying patterns of specific growth rates and cell sizes in the 2nd experiment were found to be similar to those in the 1st experiment (Table 1). Analysis of intracellular Ni content revealed over 30-fold increase within 3 orders of magnitude of Ni concentration range, while Ni quota significantly increased from 0.04 to 1.21 amol cell^{-1} with increasing Ni concentrations (Fig. 1; Table 1). The varying pattern of Ni quota, obtained from the 2nd experiment, was also found to be similar to the 1st experiment (Table 1). Other trace metal quotas were also determined (Supporting Information Table S1).

Unlike the specific growth rates and Ni quota, diel H_2 net production rates showed two distinct patterns, with relatively low net production for 2 and 20 nM treatments and relatively high net production for 0.03 and 0.2 nM treatments in the 1st experiment (Fig. 2a; Supporting Information Table S2). For the 1st experiment, H_2 net production rates for 0.03 nM treatment were 0.11, 0.12, 2.22, and 1.34 fmol H_2 cell^{-1} h^{-1} during the periods D0–D1, D1–D5, D5–D9, and D9–L1, respectively (Table 2), and similar trends were observed in the 0.2 nM treatment. However, H_2 net production rates were extremely low in the two high Ni treatments, which were 0.09, 0.04, 0.15, and 0.04 fmol H_2 cell^{-1} h^{-1} in the 2 nM treatment during the four periods, with similar rates observed in the 20 nM treatment. Compared to the rates observed during D5 and D9 periods, H_2 net production rate of the 0.2 nM treatment was 36 times higher than that of the 20 nM treatment. For the 2nd experiment, which started from the light period, H_2 net production rates in the 0.03 nM treatment were 0.04, 1.23, and 1.74 fmol H_2 cell^{-1} h^{-1} during the periods D0–D3, D3–D6, and D6–D9, respectively (Table 2). Similar trends were observed in the 0.2 nM treatment. Unlike the 1st experiment, the 2 nM treatment exhibited high H_2 net production, similar

Table 1. Ni quota (amol cell^{-1}), specific growth rate (d^{-1}), and cell size (μm^3 cell^{-1}) of *Cyanothece* obtained from the four Ni treatments in the three experiments.

$[Ni]_{total}$	Ni quota (amol cell^{-1})		Specific growth rate (d^{-1})			Cell size (μm^3 cell^{-1})		
(nM)	1st	2nd	1st	2nd	Suppl.	1st	2nd	Suppl.
0.03	0.04 ± 0.05	0.06 ± 0.02	0.60 ± 0.06	0.60 ± 0.01	0.50 ± 0.01	58 ± 11	36 ± 1	34 ± 0
0.2	0.13 ± 0.10	0.25 ± 0.07	0.72 ± 0.06	0.62 ± 0.00	0.61 ± 0.05	49 ± 4	41 ± 1	41 ± 3
2	0.31 ± 0.06	0.51 ± 0.23	0.77 ± 0.01	0.71 ± 0.01	0.72 ± 0.01	38 ± 2	37 ± 1	36 ± 1
20	1.21 ± 0.29	1.48 ± 0.67	0.79 ± 0.02	0.73 ± 0.02	0.80 ± 0.01	38 ± 2	35 ± 2	34 ± 0

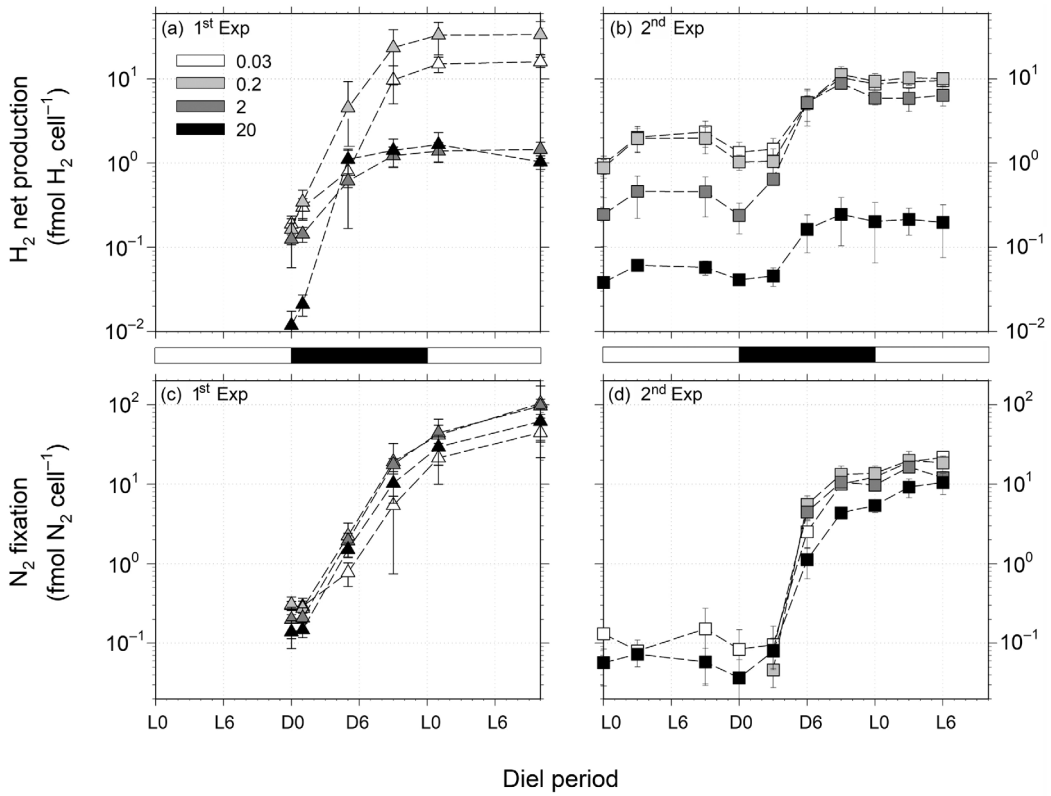

Fig. 2. Comparison of diel H_2 net production and N_2 fixation measured in two major experiments. The incubation of the 1st experiment started from dark period (D0); the incubation of the 2nd experiment started from light period (L0). (**a**,**b**) H2 net production with time obtained from the 1st and 2nd experiments. (**c**,**d**) N_2 fixation with time ($n = 3$). White and blank bars shown at the *x*-axis of plots (**a**) and (**b**) indicate the light and dark periods, respectively.

Table 2. The data of diel H_2 net production rate (fmol H_2 cell^{-1} h^{-1}) observed in the four Ni treatments of the 1st and 2nd experiments. The 1st experiment started from the dark period and lasted for 22 h. The 2nd experiment started from the light period and lasted for 30 h. The numbers noted after D or L (dark or light periods) stand for hour numbers after the start of the periods.

		H_2 net production rate, $[Ni]_{total}$			
Exp.	**Period (h)**	**0.03**	**0.2**	**2**	**20**
1st	D0–D1	0.11 ± 0.04	0.2 ± 0.1	0.086	0.014 ± 0.001
	D1–D5	0.12 ± 0.14	0.9 ± 1.1	0.04 ± 0.03	0.069
	D5–D9	2 ± 1	5 ± 3	0.15 ± 0.06	0.1 ± 0.1
	D9–L1	1.3 ± 0.4	2.4 ± 0.4	0.04 ± 0.02	0.06 ± 0.04
	L1–L10	0.1 ± 0.1	0.07 ± 0.03	0.007 ± 0.007	−0.07 ± 0.05*
2nd	L0–L3	0.4 ± 0.2	0.4 ± 0.1	0.07 ± 0.03	0.008 ± 0.002
	L3–L9	0.05 ± 0.02	0.03 ± 0.00	0.003	0.001 ± 0
	L9–L12	−0.3 ± 0.1*	−0.4 ± 0.2*	−0.07 ± 0.05*	−0.006 ± 0.003*
	D0–D3	0.04 ± 0.03	0.088	0.14 ± 0.02	0.003 ± 0.001
	D3–D6	1.2 ± 0.7	1.6 ± 0.4	1.5 ± 0.3	0.04 ± 0.02
	D6–D9	1.7 ± 0.2	2.0 ± 0.4	1.2 ± 0.2	0.03 ± 0.02
	D9–D12	−0.5 ± 0.5*	0.48	−1.0 ± 0.3*	−0.015 ± 0.002*
	L0–L3	0.2 ± 0.3	0.5 ± 0.1	0.14 ± 0.02	0.004 ± 0.021
	L3–L6	0.10 ± 0.06	0.022	0.17 ± 0.11	0.019

*Negative rates: the average H_2 concentrations of the period were slightly lower than the average concentrations of the previous period.

Table 3. The data of the diel N_2 fixation rates (fmol N_2 cell^{-1} h^{-1}) of the four Ni treatments of the 1st and 2nd experiments.

		N_2 fixation rates, $[Ni]_{total}$			
Exp.	Period (h)	0.03	0.2	2	20
1st	D0–D1	0.005	−0.03 ± 0.04*	0.017 ± 0.001	0.02 ± 0.02
	D1–D5	0.07 ± 0.09	0.6 ± 0.3	0.2 ± 0.1	0.13 ± 0.02
	D5–D9	1 ± 1	5 ± 3	3.9 ± 0.8	2.2 ± 0.7
	D9–L1	4 ± 2	10 ± 6	7 ± 2	5 ± 2
	L1–L10	3 ± 1	12 ± 8	6 ± 1	4 ± 2
2nd	L0–L3	−0.02 ± 0.02*	0.014 ± 0.005	0.03 ± 0.04	0.010 ± 0.001
	L3–L9	0.01 ± 0.02	−0.013*	0.02 ± 0.01	0.002
	L9–L12	−0.02 ± 0.02*	0.06 ± 0.005	0.04 ± 0.01	−0.007 ± 0.001*
	D0–D3	0.009 ± 0.002	0.04 ± 0.03	0.09 ± 0.02	0.01 ± 0.01
	D3–D6	0.8 ± 0.3	1.9 ± 0.5	1.5 ± 0.3	0.3 ± 0.2
	D6–D9	2.5 ± 0.2	2.6 ± 0.7	2.05 ± 0.05	1.1 ± 0.3
	D9–D12	0.7 ± 0.4	0.23 ± 0.06	0.462	0.3 ± 0.3
	L0–L3	2.3 ± 0.4	2.1 ± 0.9	2.2 ± 0.4	1.3 ± 0.5
	L3–L6	0.9 ± 0.4	0.3 ± 0.2	−1.5 ± 0.2*	0.4 ± 0.3

*Negative rates: the average ethylene concentrations of the period were slightly lower than the concentrations of the previous period.

to the 0.03 and 0.2 treatments, with the rates of 0.14, 1.53, and 1.21 for the three periods. Similar to the 1st experiment, H_2 net production in the 20 nM treatment only slightly increased during the 30-h incubation period and remained extremely low during the whole period, with the rates of 0.003, 0.04, and 0.03 fmol H_2 cell^{-1} h^{-1} during the three periods, respectively. In brief, the treatments 0.03, 0.2, and 2 nM Ni exhibited a similar pattern, where H_2 net production rapidly increased during the dark period, with the highest rate observed during D3–D9 then decreasing from D9 to L6 (Fig. 2b).

N_2 fixation rates exhibited a relatively uniform pattern among the four treatments (Fig. 2c,d; Supporting Information Table S3). For the 1st experiment, N_2 fixation rates in the 0.03 nM treatment were 0.07, 1.1, and 4.0 fmol N_2 cell^{-1} h^{-1} during the periods D1–D5, D5–D9, and D9–L1, respectively (Table 3), with similar trends observed for Ni in the 0.2, 2, and 20 nM treatments. For the 2nd experiment, N_2 fixation rates in the 0.03 nM treatment were 0.8, 2.5, and 0.7 fmol N_2 cell^{-1} h^{-1} during the periods D3–D6, D6–D9, and D9–D12, respectively (Table 3), with similar trends observed for Ni in the 0.2, 2, and 20 nM treatments. Molar ratios for daily H_2 net production to N_2 fixation rates in the 0.03 and 0.2 treatments in the 1st experiment exhibited high values, that is, 0.40 and 0.38, respectively (Table 4). In contrast, the molar ratios for daily H_2 net production to N_2 fixation rates in the 2 and 20 nM treatments were 0.015 and 0.019, respectively. Likewise, molar ratios for daily H_2 net production to N_2 fixation rates in the 0.03 and 0.2 nM treatments in the 2nd experiment exhibited high values (0.45 and 0.58, respectively). In the 2 nM treatment, the molar ratio (0.52) for daily H_2 net production to N_2 fixation observed in the 2nd experiment was substantially higher compared to the 1st experiment. The molar ratio for daily H_2 net production to N_2 fixation in the 20 nM treatment was 0.02 in the 2nd experiment.

Table 4. The molar ratios of daily H_2 net production to fixed N_2 of the four Ni treatments of the 1st and 2nd experiments.

$[Ni]_{total}$ (nM)	H_2/N_2	
	1st	2nd
0.03	0.40 ± 0.12	0.45 ± 0.06
0.2	0.38 ± 0.13	0.58 ± 0.23
2	0.015 ± 0.002	0.52 ± 0.10
20	0.019 ± 0.007	0.02 ± 0.02

Discussion

Effects of Ni on H_2 net production and N_2 fixation

Among the four Ni treatments, the diel H_2 net production exhibited two distinct patterns: relatively low net production for the two high Ni treatments and relatively high net production for the two low Ni treatments in the 1st experiment (Fig. 2a). A similar two-pattern trend in H_2 net production was also observed in the 2nd experiment, with 2 nM treatment close to the results observed for the two low Ni treatments (Fig. 2b). However, the diel variations for both N_2 fixation rates and NifH expression were comparable in all four treatments (Figs. 2c,d, 3). It is noteworthy that comparable N_2 fixation rates would result in similar H_2 gross production. Thus, the observed high H_2 net production can be attributed to low HupL expression under limited Ni conditions, whereas low

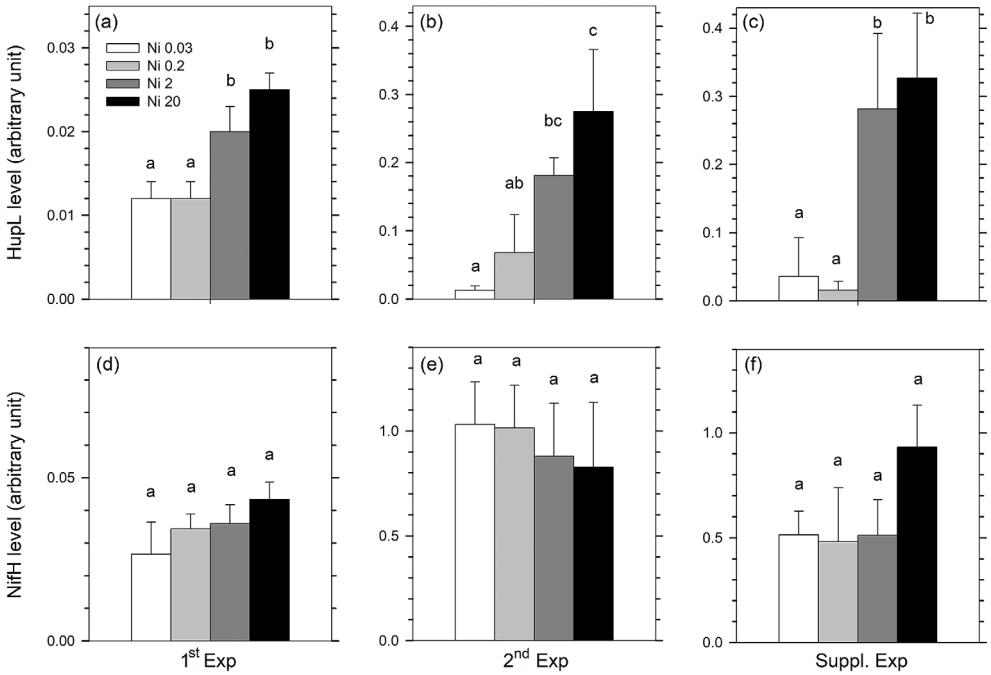

Fig. 3. Comparisons of the protein expression levels of uptake hydrogenase and nitrogenase among the four Ni treatments in the three experiments. The two proteins were determined by their subunits HupL and NifH with Western blotting approach. (**a**–**c**) HupL level normalized to total protein (**a**) (ANOVA, $F_{3,8} = 23.2$, $p < 0.001$) (**b**) (ANOVA, $F_{3,8} = 16.0$, $p < 0.001$) (**c**) (ANOVA, $F_{3,8} = 14.9$, $p < 0.01$). (**d**–**f**) NifH level normalized to total protein. The expression levels of HupL and NifH in the 1st experiment were significantly lower than the value observed in the other two experiments. As Western blotting approach is a semi-quantitative method, several factors may vary significantly among different batch experiments and thus result in significant differences in target protein expression levels among different batch experiments. The factors include the transfer efficiency of proteins, the aggregation of target proteins, the exposure of protein image, and the quantification of total proteins. The comparison of the protein levels should be limited to each experiment.

production can be attributed to high H_2 uptake by high HupL expression under abundant Ni conditions (Fig. 3).

In terms of the diel variations of N_2 fixation, N_2 fixation substantially increased during the dark period in the first experiment (Fig. 2c). *Cyanothece*, a non-heterocystous cyanobacterium, is expected to fix N_2 only during the dark period since nitrogenase is sensitive to oxygen (Bergman et al. 1997). However, we observed that N_2 fixation seemed to continue to increase after the dark period in both experiments (Fig. 2; Table 2). Previous studies have reported that nitrogenase RNA and NifH protein were overexpressed during the dark period, and their abundance was relatively low during the light period (Colón-López et al. 1997; Aryal et al. 2013). Bandyopadhyay et al. (2010) reported a clear absence of *nifH* expression after 1-h light exposure. By applying a 24-h constant light condition, Colón-López et al. (1997) identified relatively high and constant N_2 fixation rates. Some other studies considered varying light–dark regimes and showed that N_2 fixation in *Cyanothece* may be extended to the light period (Rabouille et al. 2014; Polerecky 2021). Bergman et al. (1997) proposed that nitrogenase may be protected by Fe protein to relieve O_2 stress during the light period. In this study, although N_2 fixation continued to increase after the dark period, H_2 net production in the 0.03 and 0.2 treatments did not increase during the light period, suggesting relatively low N_2 fixation activity during the light period. We suspected that the increase in N_2 fixation after the dark period may be an artifact. Thus, we carried out the 30-h 2nd experiment by starting N_2 fixation measurements from the light period to examine N_2 fixation rates. In the 2nd experiment, we found that the fixed N_2 remained extremely low during the first 12 h (L0–D0), with no signs of N_2 fixation activity at the beginning of the first light period (Fig. 2d). The elevated N_2 fixation values observed after the dark period in both experiments were likely to be artifacts, which might be attributed to the lag period effect, driven by nitrogen starvation due to the relatively long assay time (Capone and Montoya 2001).

H_2/N_2 ratios and Ni threshold

It is expected that the molar ratios of H_2 net production to N_2 fixation rates (hereafter H_2/N_2 ratio) should be close to one under conditions of deficient Ni availability or uptake hydrogenase expression; the ratios are expected to be closer to 0 with ample Ni supply to synthesize uptake hydrogenase (Fig. 3). In the 1st experiment, we did identify two prominent H_2 net production patterns between the two low- and two high-Ni

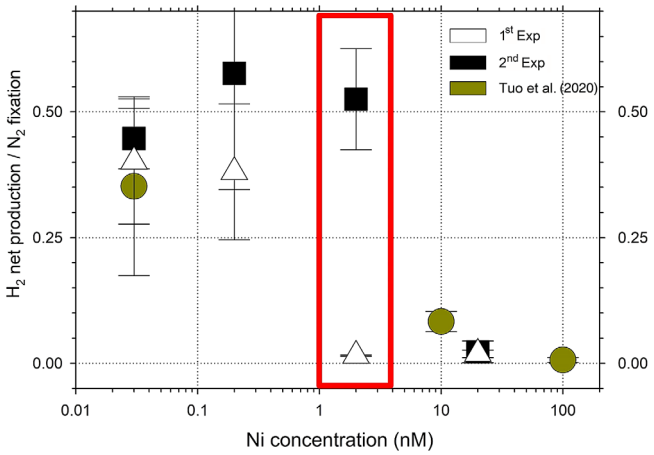

Fig. 4. Comparison of the ratios of daily H_2 net production to fixed N_2 obtained from the 1st and 2nd experiments and Tuo et al. (2020), which are presented by the symbols of triangle, square, and circle, respectively. The red highlighted zone indicates a speculative range of the Ni threshold concentration which results in two distinctive ratios. The ratios of the two lowest Ni treatments (0.03 and 0.2 nM) were significant different from the two highest treatments (20 and 100 nM) among the treatments across different experiments (ANOVA, $F_{5,26} = 13.3$, $p < 0.001$). There is no statistical difference within the same Ni concentration between 1st and 2nd experiments except for Ni 2 treatment (ANOVA, $F_{1,4} = 77.0$, $p < 0.001$). The time frames used to calculate the ratios are 22 and 30 h for our 1st and 2nd experiments, respectively and only 12 h in dark period for the study of Tuo et al. (2020) (Table 5).

treatments. The 2 and 20 nM treatments exhibited relatively low H_2 net production; the 0.03 and 0.2 nM treatments exhibited relatively high production. Thus, the ratios for the two high Ni treatments were extremely low (0.015 and 0.019, respectively), while the ratios for the two low Ni treatments were 0.40 and 0.38, respectively (Fig. 4, Table 4). The results of the 2nd experiment were similar to those of the 1st experiment, with an exception of 2 nM treatment. The H_2 net production pattern of the 2 nM treatment was comparable to that of the two low Ni treatments (Fig. 4).

As Tuo et al. (2020) conducted a similar experiment with shorter time duration for the measurement of N_2 fixation and H_2 production, we have compared our data with the data of Tuo et al. (2020). Most observations of the parameters, including Ni quota, specific growth rates, and H_2/N_2 ratios, were comparable between the two studies (Table 5). However, Tuo et al. (2020) showed a negative correlation between N_2 fixation rate and Ni supply even though the correlation was not particularly strong (Figs. 5, 6). As this study carried out time course experiments lasting 22 or 30 h and demonstrated good precision for N_2 fixation rates (Fig. 2), the N_2 fixation data obtained in this study can be considered highly reliable.

Based on the consistent molar ratios observed in these two studies, we suggest that the threshold Ni concentration for inducing significant expression of uptake hydrogenase is ~2 nM for the culture conditions used in this study (Fig. 4). It should be noted that the Ni levels mentioned here were operationally defined in this culture study, representing total dissolved concentrations in the medium with 20 μM EDTA. Bioavailable Ni concentrations in this culture study are not equivalent to the total dissolved Ni concentrations observed in the field.

Hydrogenase and nitrogenase expression

Total protein normalized HupL levels were generally related to Ni availability, with significantly higher expression levels in the two high Ni treatments than in the two low Ni treatments (Fig. 3; Supporting Information Fig. S3; Table S4). In the 2nd experiment, the expression levels in the two high Ni treatments were about one order of magnitude higher than the levels observed in the two low Ni treatments (Fig. 3). Compared to the results of the 2nd experiment, the expression levels for both HupL and NifH were relatively low in the 1st experiment, possibly due to a quantification problem for total protein. We thus carried out an additional experiment to examine the protein levels. In the additional (supplementary) experiment, the protein levels of HupL in the two high Ni treatments were comparable to the values observed in the 2nd experiment and were also much higher than the values observed in the two low-Ni treatments (Fig. 3), indicating that the HupL levels expressed reflected the activities of hydrogenase for H_2 uptake. In

Table 5. Comparisons of Ni quota, specific growth rate, and daily H_2/N_2 ratio between this study and Tuo et al. (2020).

$[Ni]_{total}$	Ni quota (amol cell^{-1})		Specific growth rate (d^{-1})		H_2/N_2 (molar ratio)	
(nM)	This study	Tuo et al.*	This study	Tuo et al.	This study	Tuo et al.
0.03	0.05 ± 0.01	0.08 ± 0.03	0.57 ± 0.06	0.63 ± 0.04	0.43 ± 0.04	0.35 ± 0.18
0.2	0.19 ± 0.08	n.a.	0.65 ± 0.06	n.a.	0.48 ± 0.14	n.a.
2	0.41 ± 0.14	n.a.	0.73 ± 0.03	n.a.	0.27 ± 0.36	n.a.
10	n.a.	0.34 ± 0.04	n.a.	0.73 ± 0.02	n.a.	0.08 ± 0.020
20	1.35 ± 0.19	n.a.	0.78 ± 0.04	n.a.	0.02 ± 0.00	n.a.
100	n.a.	1.42 ± 0.03	n.a.	0.73 ± 0.08	n.a.	0.007 ± 0.005

n.a., not available.
*The Ni treatments of the study of Tuo et al. (2020) were 0.03, 10, and 100 nM.

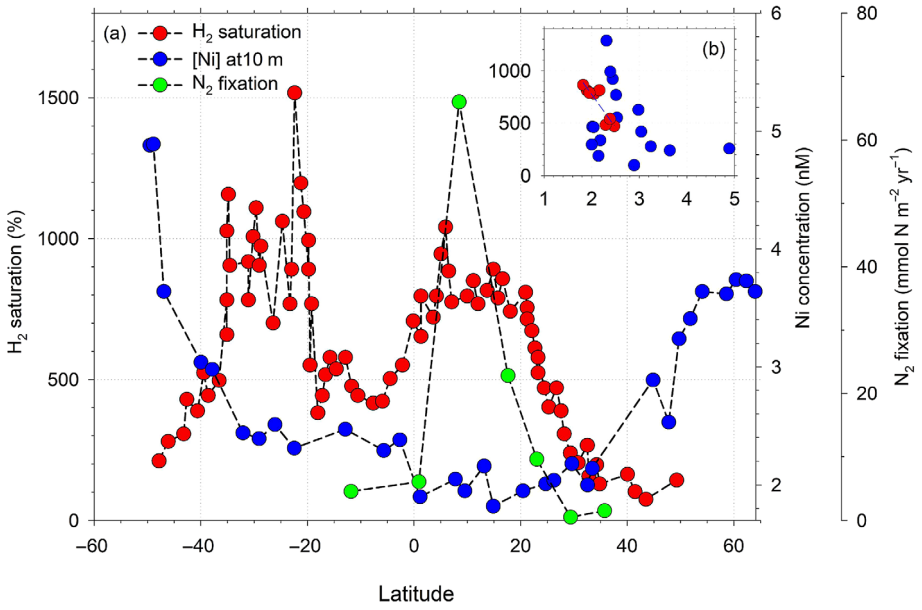

Fig. 5. Comparison of H_2 saturation percentage with dissolved Ni concentrations in the surface water of the Atlantic Ocean (**a**) Ni concentration (blue dots), H_2 saturation (red dots), and N_2 fixation flux (green dots) plotted along two meridional transects in the Atlantic Ocean. H_2 saturation data and N_2 fixation were extracted from fig. 2a in Moore et al. (2014) by using WebPlotDigitizer 4.4. Ni concentration data were obtained from the GEOTRACES Intermediate Data Product 2017 (Schlitzer et al. 2018). (**b**) The correlation between H_2 saturation percentage and dissolved Ni concentrations for the 32 Ni samples. H_2 data were chosen by closest sampling sites to the Ni sampling sites in terms of latitude. The data show significant negative correlation (Spearman's correlation, $n = 25$, $rs = -0.40$, $p < 0.05$). Red dots shown in (**b**) stand for the samples within 20°N and 20°S (Spearman's correlation, $n = 8$, $rs = -0.83$, $p < 0.05$). It should be noted that the transects of two independent cruises were not aligned and sampling sites at the same latitude are subjected to a 15° longitude difference on average.

addition, the HupL levels in the two low Ni treatments were still detectable, suggesting that HupL was expressed at a relatively low level to take up H_2 under extremely low Ni conditions. These results explain why the H_2/N_2 ratios were still less than 1 in the two low Ni treatments.

Consistent with the N_2 fixation rates observed among the different Ni treatments (Fig. 2c,d), expression levels of NifH were also comparable among the four Ni treatments in all three experiments (Fig. 3; Supporting Information Table S4), proving that NifH expression was not affected by Ni availability and HupL levels. These results do not support the argument of Zhang et al. (2014) that HupL protects nitrogenase from O_2 stress in *Cyanothece*, but support the argument of Daday et al. (1985) that no significant decrease in N_2 fixation activity was observed under low Ni conditions.

H_2 production and Ni availability in the euphotic zone

Overall, the findings of this study suggest that Ni availability is a major factor affecting H_2 net production and its concentration levels in the euphotic zone of the oceans. High N_2 fixation rates yield high H_2 gross production, but Ni availability further affects H_2 net production or its saturation percentage in the surface water of tropical and subtropical oceans. Attributed to GEOTRACES project, Ni concentrations are available for us to examine their correlation with H_2 concentrations reported previously (Moore et al. 2014; Schlitzer et al. 2018; Middag et al. 2020). It should be noted that dissolved Ni concentrations in the surface water in the tropical and subtropical regions of both the Atlantic and Pacific Oceans are relatively low and consistent, with the values of ~2 nM (Schlitzer et al. 2018; Middag et al. 2020; Zheng et al. 2021). The study of Middag et al. (2020) reported Ni concentrations in the surface water of the western Atlantic Ocean, located between 64°N and 49°S, and sampled from April to July 2010 and March to April 2011 (Middag et al. 2020). The lowest concentrations were found at 0–25°N, with a concentration of ~2 nM (Fig. 5). In the southern tropical and subtropical regions, the concentrations were estimated to be ~2.5 nM. In another study (Moore et al. 2014), H_2 concentrations and saturation percentages were measured from October to November 2010. H_2 concentrations were relatively high in the tropical and subtropical waters, particularly in the regions of 0–20°N and 20–35°S (Fig. 5). N_2 fixation rates were measured discretely on the same cruise from 35°N to 10°S, also exhibiting the highest fluxes at 0–20°N, where H_2 saturation percentages were relatively high (Fig. 5; Moore et al. 2014). These significant correlations between dissolved Ni concentration, N_2 fixation, and H_2 saturation percentage suggest that Ni availability may be a major factor affecting diazotrophic H_2 net

production and its saturation percentage in the oceanic water when Ni concentrations are relatively low.

This study proved that low Ni availability yields low hydrogenase expression levels and high H_2 net production in a model unicellular diazotrophic cyanobacterium, *Cyanothece*. The results indicate that low Ni availability and high H_2 net production did not affect nitrogenase expression levels and N_2 fixation rates in *Cyanothece*. This study also identified the threshold level of Ni concentrations that may induce contrasting levels of HupL and H_2 net production in the cells. The significant correlation between Ni and H_2 concentrations observed in surface water of the tropical and subtropical regions of the Atlantic Ocean supports the finding of this culture study that Ni availability may be an important factor influencing biological H_2 net production in oceans.

Data availability statement

All of the data are available at the tables of the main text and the Supporting Information.

References

Aryal, U. K., and others. 2013. Proteome analyses of strains ATCC 51142 and PCC 7822 of the diazotrophic cyanobacterium *Cyanothece* sp. under culture conditions resulting in enhanced H_2 production. Appl. Environ. Microbiol. **79**: 1070–1077. doi:10.1128/AEM.02864-12

Axelsson, R., and P. Lindblad. 2002. Transcriptional regulation of *Nostoc* hydrogenases: Effects of oxygen, hydrogen, and nickel. Appl. Environ. Microbiol. **68**: 444–447. doi:10.1128/AEM.68.1.444-447.2002

Bandyopadhyay, A., J. Stöckel, H. Min, L. A. Sherman, and H. B. Pakrasi. 2010. High rates of photobiological H_2 production by a cyanobacterium under aerobic conditions. Nat. Commun. **1**: 139. doi:10.1038/ncomms1139

Bergman, B., J. R. Gallon, A. N. Rai, and L. J. Stal. 1997. N_2 fixation by non-heterocystous cyanobacteria. FEMS Microbiol. Rev. **19**: 139–185.

Bothe, H., O. Schmitz, M. G. Yates, and W. E. Newton. 2010. Nitrogen fixation and hydrogen metabolism in cyanobacteria. Microbiol. Mol. Biol. Rev. **74**: 529–551. doi:10.1128/MMBR.00033-10

Bruland, K. W. 1980. Oceanographic distributions of cadmium, zinc, nickel, and copper in the North Pacific. Earth Planet. Sci. Lett. **47**: 176–198. doi:10.1016/0012-821X(80)90035-7

Burnette, W. N. 1980. "Western blotting": Electrophoretic transfer of proteins from sodium dodecyl sulfate-polyacrylamide gels to unmodified nitrocellulose and radiographic detection with antibody and radioiodinated protein A. Anal. Biochem. **112**: 195–203. doi:10.1016/0003-2697(81)90281-5

Capone, D. G., and J. P. Montoya. 2001. Nitrogen fixation and denitrification. Methods Microbiol. **30**: 501–515. doi:10.1016/s0580-9517(01)30060-0

Colón-López, M. A., D. M. Sherman, and L. A. Sherman. 1997. Transcriptional and translational regulation of nitrogenase in light-dark- and continuous-light-grown cultures of the unicellular cyanobacterium *Cyanothece* sp. strain ATCC 51142. J. Bacteriol. **179**: 4319–4327. doi:10.1128/jb.179.13.4319-4327.1997

Daday, A., and G. D. Smith. 1983. The effect of nickel on the hydrogen metabolism of the cyanobacterium *Anabaena cylindrica*. FEMS Microbiol. Lett. **20**: 327–330.

Daday, A., A. H. Mackerras, and G. D. Smith. 1985. The effect of nickel on hydrogen metabolism and nitrogen fixation in the cyanobacterium *Anabaena cylindrica*. J. Gen. Microbiol. **131**: 231–238.

Dixon, R. O. D. 1972. Hydrogenase in legume root nodule bacteroids: Occurrence and properties. Arch. Mikrobiol. **85**: 193–201. doi:10.1007/BF00408844

Dupont, C. L., K. Barbeau, and B. Palenik. 2008. Ni uptake and limitation in marine *Synechococcus* strains. Appl. Environ. Microbiol. **74**: 23–31. doi:10.1128/AEM.01007-07

Eichner, M., S. Basu, M. Gledhill, D. de Beer, and Y. Shaked. 2019. Hydrogen dynamics in *Trichodesmium* colonies and their potential role in mineral iron acquisition. Front. Microbiol. **10**: 1565. doi:10.3389/fmicb.2019.01565

Guth, J. H., and R. H. Burris. 1983. Inhibition of nitrogenase-catalyzed NH_3 formation by H_2. Biochemistry **22**: 5111–5122. doi:10.1021/bi00291a010

Herr, F. L., and W. R. Barger. 1978. Molecular hydrogen in the near-surface atmosphere and dissolved in waters of the tropical North Atlantic. J. Geophys. Res. Oceans **83**: 6199–6205. doi:10.1029/JC083iC12p06199

Ho, T. Y. 2013. Nickel limitation of nitrogen fixation in *Trichodesmium*. Limnol. Oceanogr. **58**: 112–120. doi:10.4319/lo.2013.58.1.0112

Ho, T. Y., A. Quigg, Z. V. Finkel, A. J. Milligan, K. Wyman, P. G. Falkowski, and F. M. M. Morel. 2003. The elemental composition of some marine phytoplankton. J. Phycol. **39**: 1145–1159. doi:10.1111/j.0022-3646.2003.03-090.x

Ho, T. Y., C. T. Chien, B. N. Wang, and A. Siriraks. 2010. Determination of trace metals in seawater by an automated flow injection ion chromatograph pretreatment system with ICPMS. Talanta **82**: 1478–1484. doi:10.1016/j.talanta.2010.07.022

Middag, R., H. J. W. de Baar, K. W. Bruland, and S. M. A. C. van Heuven. 2020. The distribution of nickel in the West-Atlantic Ocean, its relationship with phosphate and a comparison to cadmium and zinc. Front. Mar. Sci. **7**: 105. doi:10.3389/fmars.2020.00105

Moore, R. M., S. Punshon, C. Mahaffey, and D. Karl. 2009. The relationship between dissolved hydrogen and nitrogen fixation in ocean waters. Deep Sea Res. Part I **56**: 1449–1458. doi:10.1016/j.dsr.2009.04.008

Moore, R. M., M. Kienast, M. Fraser, J. J. Cullen, C. Deutsch, S. Dutkiewicz, M. J. Follows, and C. J. Somes. 2014. Extensive hydrogen supersaturations in the western South Atlantic Ocean suggest substantial underestimation of nitrogen fixation. J. Geophys. Res. Oceans **119**: 4340–4350. doi:10.1002/2014JC010017

Moore, R. M., I. Grefe, J. Zorz, S. Shan, K. Thompson, J. Ratten, and J. LaRoche. 2018. On the relationship between hydrogen saturation in the tropical Atlantic Ocean and nitrogen fixation by the symbiotic diazotroph UCYN-A. J. Geophys. Res. Oceans **123**: 2353–2362. doi:10.1002/2017JC013047

Polerecky, L., and others. 2021. Temporal patterns and intra- and inter-cellular variability in carbon and nitrogen assimilation by the unicellular cyanobacterium *Cyanothece* sp. ATCC 51142. Front. Microbiol. **12**: 620915. doi:10.3389/fmicb.2021.620915

Price, N. M., and F. M. M. Morel. 1991. Colimitation of phytoplankton growth by nickel and nitrogen. Limnol. Oceanogr. **36**: 1071–1077. doi:10.4319/lo.1991.36.6.1071

Punshon, S., and R. M. Moore. 2008. Aerobic hydrogen production and dinitrogen fixation in the marine cyanobacterium *Trichodesmium erythraeum* IMS101. Limnol. Oceanogr. **53**: 2749–2753. doi:10.4319/lo.2008.53.6.2749

R Core Team. 2021. R: A language and environment for statistical computing. R Foundation for Statistical Computing.

Rabouille, S., D. B. Van de Waal, H. C. P. Matthijs, and J. Huisman. 2014. Nitrogen fixation and respiratory electron transport in the cyanobacterium *Cyanothece* under different light/dark cycles. FEMS Microbiol. Ecol. **87**: 630–638. doi:10.1111/1574-6941.12251

Rodriguez, I. B., and T. Y. Ho. 2014. Diel nitrogen fixation pattern of *Trichodesmium*: The interactive control of light and Ni. Sci. Rep. **4**: 4445. doi:10.1038/srep04445

Saito, M. A., J. W. Moffett, and G. R. DiTullio. 2004. Cobalt and nickel in the Peru upwelling region: A major flux of labile cobalt utilized as a micronutrient. Global Biogeochem. Cycl. **18**: GB4030. doi:10.1029/2003GB002216

Schlitzer, R., and others. 2018. The GEOTRACES intermediate data product 2017. Chem. Geol. **493**: 210–223. doi:10.1016/j.chemgeo.2018.05.040

Schmidt, U., and W. Seiler. 1970. A new method for recording molecular hydrogen in atmospheric air. J. Geophys. Res. **75**: 1713–1716.

Schropp, S. J., M. I. Scranton, and J. R. Schwarz. 1987. Dissolved hydrogen, facultatively anaerobic, hydrogen-producing bacteria, and potential hydrogen production rates in the western North Atlantic Ocean and Gulf of Mexico. Limnol. Oceanogr. **32**: 396–402. doi:10.4319/lo.1987.32.2.0396

Scranton, M. I. 1984. Hydrogen cycling in the waters near Bermuda: The role of the nitrogen fixer, *Oscillatoria thiebautii*. Deep-Sea Res., Part A **31**: 133–143. doi:10.1016/0198-0149(84)90020-7

Setser, P. J., J. L. Bullister, E. C. Frank, N. L. Guinasso, and D. R. Schink. 1982. Relationships between reduced gases, nutrients, and fluorescence in surface waters off Baja California. Deep-Sea Res. Part A **29**: 1203–1215. doi:10.1016/0198-0149(82)90090-5

Tuo, S. H., I. B. Rodriguez, and T. Y. Ho. 2020. H_2 accumulation and N_2 fixation variation by Ni limitation in *Cyanothece*. Limnol. Oceanogr. **65**: 377–386. doi:10.1002/lno.11305

Volbeda, A., M. H. Charon, C. Piras, E. C. Hatchikian, M. Frey, and J. C. Fontecilla-Camps. 1995. Crystal structure of the nickel-iron hydrogenase from *Desulfovibrio gigas*. Nature **373**: 580–587. doi:10.1038/373580a0

Wang, B. S., C. P. Lee, and T. Y. Ho. 2014. Trace metal determination in natural waters by automated solid phase extraction system and ICP-MS: The influence of low level Mg and Ca. Talanta **128**: 337–344. doi:10.1016/j.talanta.2014.04.077

Wilson, S. T., R. A. Foster, J. P. Zehr, and D. M. Karl. 2010. Hydrogen production by *Trichodesmium erythraeum*, *Cyanothece* sp., and *Crocosphaera watsonii*. Aquat. Microb. Ecol. **59**: 197–206. doi:10.3354/ame01407

Zhang, X., D. M. Sherman, and L. A. Sherman. 2014. The uptake hydrogenase in the unicellular diazotrophic cyanobacterium *Cyanothece* sp. strain PCC 7822 protects nitrogenase from oxygen toxicity. J. Bacteriol. **196**: 840–849. doi:10.1128/JB.01248-13

Zheng, L., T. Minami, S. Takano, T.-Y. Ho, and Y. Sohrin. 2021. Sectional distribution patterns of Cd, Ni, Zn, and Cu in the North Pacific Ocean: Relationships to nutrients and importance of scavenging. Global Biogeochem. Cycl. **35**: e2020GB006558. doi:10.1029/2020GB006558

Acknowledgments

The authors appreciate the technical assistance by C.-C. Chen, C.-C. Hsieh, H.-C. Chu, L.-W. Zeng, and S. Null. The authors thank anonymous reviewers for their constructive comments. This study was financially supported by grants MOST 108-2611-M-001-006-MY3 and 108-2923-M-001-009-MY3 from Taiwan Ministry of Science and Technology and by Investigator Award AS-IA-110-M03 from Academia Sinica to T.-Y. Ho.

Conflict of interest

The authors have no conflicts of interest to declare.

Submitted 10 August 2021
Revised 20 April 2022
Accepted 04 May 2022

Editor-in-Chief: K. David Hambright